FEBS Open Bio 5 (2015) 76–84

journal homepage: www.elsevier.com/locate/febsopenbio

Ligand binding specificity of RutR, a member of the TetR family of transcription regulators in *Escherichia coli*

Phu Nguyen Le Minh [a,b], Sergio de Cima [b], Indra Bervoets [a], Dominique Maes [c], Vicente Rubio [b], Daniel Charlier [a,*]

[a] Research Group of Microbiology, Vrije Universiteit Brussel (VUB), Pleinlaan 2, B-1050 Brussel, Belgium
[b] Instituto de Biomedicina de Valencia del Consejo Superior de Investigaciones Cientificas (IBV-CSIC), Centro de Investigación Biomédicaen Red de Enfermedades Raras (CIBERER-ISCIII), C/Jaime Roig 11, E-46010 Valencia, Spain
[c] Structural Biology Brussels, Vrije Universiteit Brussel (VUB), Pleinlaan 2, B-1050 Brussel, Belgium

ARTICLE INFO

Article history:
Received 5 January 2015
Revised 14 January 2015
Accepted 14 January 2015

Keywords:
carAB
Arginine biosynthesis
Pyrimidine biosynthesis
Carbamoylphosphate
Protein–DNA interactions
Crystallography

ABSTRACT

RutR is a member of the large family of TetR transcriptional regulators in *Escherichia coli*. It was originally discovered as the regulator of the *rutABCDEFG* operon encoding a novel pathway for pyrimidine utilization, but its highest affinity target is the control region of the *carAB* operon, encoding carbamoylphosphate synthase. Unlike most other TetR-like regulators, RutR exerts both positive and negative effects on promoter activity. Furthermore, RutR exhibits a very narrow ligand binding specificity, unlike the broad effector specificity that characterizes some of the well-studied multidrug resistance regulators of the family. Here we focus on ligand binding and ligand specificity of RutR. We construct single alanine substitution mutants of amino acid residues of the ligand-binding pocket, study their effect on *in vitro* DNA binding in absence and presence of potential ligands, and analyse their effect on positive regulation of the *car*P1 promoter and negative autoregulation *in vivo*. Although RutR structures have been determined previously, they were deposited in the Protein Data Bank without accompanying publications. All of them have uracil bound in the effector-binding site, representing the inactive form of the regulator. We determined the crystal structure of an unliganded mutant RutR protein and provide a structural basis for the use of uracil as sole effector molecule and the exclusion of the very similar thymine from the ligand-binding pocket.

1. Introduction

Escherichia coli RutR (b1013, *ycdC*) is a two-domain transcriptional regulator that belongs to the TetR family [1]. These one-component signal transduction systems are particularly abundant in bacteria and archaea that thrive in biotopes with frequent changes in nutrient composition. TetR-like regulators are involved in transcriptional control of a multitude of systems and pathways, including multidrug resistance, production of antibiotics, pathogenicity, quorum sensing, osmotic stress, biofilm formation, cytokinesis, and various pathways, mainly catabolic [2–6]. Due to its tight regulation TetR, the well-studied archetype of the family, is commonly used as a genetic control element to selectively regulate heterologous gene expression, also in eukaryotes [7]. However, the physiological function and ligand(s) of most other family members are not known. TetR-like proteins exhibit a high degree of sequence conservation in the N-terminal DNA-binding region, but a very low conservation in the rest of the molecule. The latter likely reflects the huge ligand diversity of TetR proteins, which furthermore frequently exhibit broad ligand specificity. Nevertheless, global structural conservation can be observed within the family, in spite of a low degree of amino acid sequence conservation [3,5]. All TetR-like regulators of which the function is known bind their target in the apo-form, whereas ligand binding results in dissociation of protein–DNA complexes. However, this can be reversed by mutation as indicated by reverse TetR, a mutant of class B TetR, which shows increased rather than decreased affinity for its operator upon ligand binding [8].

RutR was originally identified as the regulator of a novel pathway for pyrimidine utilization, encoded by the *rutABCDEFG* operon [1,9,10]; later on its genome-wide binding profile was determined

* Corresponding author at: Research Group of Microbiology, Department of Bioengineering Sciences, Vrije Universiteit Brussel (VUB), Pleinlaan 2, B-1050 Brussel, Belgium. Tel.: +32 2 6291342; fax: +32 2 6291345.
E-mail addresses: nguyenleminh.phu@gmail.com (P. Nguyen Le Minh), sergiodecima@ibv.csic.es (S. de Cima), indra.bervoets@vub.ac.be (I. Bervoets), Dominique.Maes@vub.ac.be (D. Maes), rubio@ibv.csic.es (V. Rubio), dcharlie@vub.ac.be (D. Charlier).

http://dx.doi.org/10.1016/j.fob.2015.01.002
2211-5463/

[11]. In striking contrast to most other bacterial transcriptional regulators, only six out of the twenty experimentally identified RutR binding sites are located in intergenic regions, and of these, five were shown to have a regulatory function (*carAB*, *rutR-rutABC-DEFG*, *gadAXW*, *gadBC*, *gcl-hyi-glxR-ybbVW-allB-ybbY-glxK*) [9,11,12]. Thus, RutR is involved in the regulation of degradation and synthesis of pyrimidines, degradation of purines, glutamine supply and pH homeostasis. The best-studied and highest affinity target of RutR is the *carAB* operon encoding carbamoylphosphate synthase. RutR binds to a semi-palindromic 15 bp conserved site positioned far upstream (centred around position −184.5) of the start of *car*P1 transcription [9,12]. Previously some of us have proposed a model for the RutR-*car*P1 complex [12] that is based on high-resolution contact mapping and saturation mutagenesis of the operator, and the similarity of RutR with the multidrug-binding QacR protein of *Staphylococcus aureus*, for which a DNA-bound co-crystal structure is available [13].

With only few exceptions, TetR family members act as repressors in the unliganded state. In contrast, apo-RutR both stimulates and inhibits gene expression at different promoters [9], but the molecular mechanisms of RutR-mediated positive and negative control are not known. Many TetR-like regulators bind hydrophobic or ring-containing molecules as inducing ligand, frequently with broad specificity [4]. Uracil and thymine have previously been proposed to modulate the DNA binding affinity of RutR [9], but the latter was not confirmed in an independent study [12].

Here, we construct single alanine substitution mutants of the effector binding-pocket of RutR, study their effects on effector binding and effector specificity *in vitro* and on *car*P1 promoter activity *in vivo*. Furthermore, we provide a structural basis for the strict ligand specificity of RutR and determine the structure of an unliganded mutant RutR protein, providing evidence of how the effector-binding signal is transmitted between domains.

2. Results

2.1. In silico identification of RutR residues important for ligand binding and ligand selectivity

Members of the TetR family are "T-shaped" homodimers. Each subunit consists of two domains, a conserved N-terminal domain with a helix-turn-helix (HTH) motif that is responsible for binding to DNA (therefore also called DBD domain), and a highly variable (in terms of primary sequence) C-terminal regulatory domain, usually also formed exclusively by helices. The latter is responsible for dimerization and effector binding (named LBD or ligand binding domain). We examined a PDB-deposited RutR structure (PDB: 4JYK; without comment or publication), finding that it shares the canonical fold of the TetR family [4], with a DBD domain of 62 amino acids that is formed by three helixes with a HTH DNA-binding motif (helices α2 and α3), and a 150 residues LBD domain formed by the six conserved helices present in all members of the family plus a seventh short helix (helix α8a) inserted between helices α8 and α9. This helix is located at the dimer interface and is part of the ligand-binding pocket (Fig. 1a).

The crystal structure of RutR, determined at 2.4 Å resolution, was first deposited in the PDB, as a result of a structural genomics study but without comment or publication, in 2003 (PDB: 1PB6),

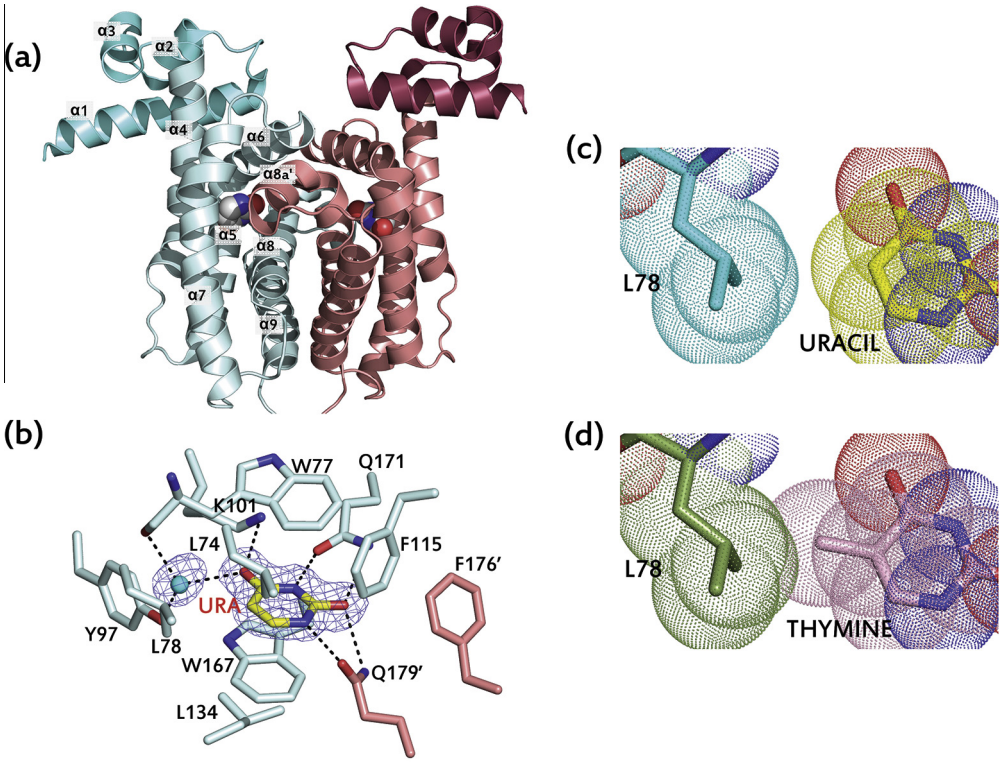

Fig. 1. Structure of uracil-bound RutR. (a) Cartoon presentation of wild type RutR dimer (PDB 4JYK). Two different hues of cyan or salmon are used to identify the DBD and LBD domains of both subunits. Helices α1 to α9 are labelled in one subunit (although, for better visualization, the labelled α8a helix is from the adjacent subunit). The uracil molecule bound to each subunit is shown as spheres. (b) Detailed view of the uracil-binding site. Protein and ligand are shown in stick representation, with the C atoms coloured in yellow for uracil, cyan for residues of one subunit, and salmon for residues of the adjacent subunit. A water molecule is shown as a cyan sphere. The Fo-Fc electron density map, calculated omitting the uracil and water molecules from the model (omit map) and contoured at 2.5σ, is shown as a blue grid. Residues involved in uracil biding are labelled. (c) Detail of the ligand-binding site showing uracil and Leu78 as sticks and clouds of dots (corresponding to Van der Waals spheres). (d) Same as (c), with thymine replacing uracil. (For interpretation of the references to colour in this figure legend, the reader is referred to the web version of this article.)

even before the function of the protein was known. Despite the presence of an evident density in the binding pocket, no ligand had been modelled in this structure. Later on a revised model including uracil bound to the pocket was deposited (PDB: 3LOC), superseding the original deposition. More recently a structure of RutR at higher resolution (1.7 Å) was deposited (PDB: 4JYK), also including a uracil molecule in the ligand-binding pocket. Apparently uracil had not been included in the crystallization solutions, and thus this nucleobase appears to have co-purified and co-crystallized with the overexpressed protein, suggesting a high affinity of RutR for uracil. This observation was corroborated by a third structure of uracil-bound wild-type RutR obtained in our laboratory (data not shown).

The structure of liganded RutR shows that uracil binds to the LBD in a pocket formed by helices α4, α5, α7 and α8, and closed at the top by helix α6 and by helix α8a of the adjacent subunit (Fig. 1a). On the one hand the binding of uracil involves a network of hydrogen bond contacts: N1 and O2 with OE1 and NE2 of Gln179 from the other subunit; O2 and N3 with OE1 and NE2 of Gln171; O4 with NZ of Lys101 and two water mediated contacts with the phenolic O atom of Tyr79 and main chain O of Trp77 (Fig. 1b). On the other hand the uracil molecule is stacked by hydrophobic interactions above and below with the aromatic rings of residues Trp77 and Trp167. In addition, the side chains of leucine residues Leu74, Leu78 and Leu134 help in fixing the aromatic ring of uracil (Fig. 1b). Furthermore, we hypothesized that Leu78 is important in ligand selectivity, as modelling of a thymine molecule in the binding site produces a steric clash between Leu78 and the C5-methyl group of the nucleobase (Fig. 1c and d). To test this hypothesis we performed site-directed mutagenesis studies of the residues Leu 74, Trp77, Leu78 and Trp167 and evaluated their importance in ligand binding and selectivity. To this end we performed *in vitro* DNA-binding assays with purified RutR proteins in absence and presence of uracil or thymine, and analysed positive and negative regulatory effects *in vivo*.

2.2. Effects of single alanine substitutions in RutR on in vitro DNA binding activity of RutR

Previously we have shown that high affinity binding of RutR to the *car*P1 control region is inhibited in the presence of uracil, whereas thymine has little or no effect [12]. This contrasts with an earlier observation [9] and suggests that thymine might be selectively excluded from the effector-binding site. Comparative EMSAs with wild-type and mutant RutR proteins binding to a 116 bp *car*P1 operator fragment, performed in absence and presence of increasing concentrations of uracil or thymine indicated that binding of RutR-W77A and RutR-W167A is similar with and without uracil, even at mM concentrations of the ligand (Fig. 2a–c). In contrast, DNA binding of RutR-L78A was still sensitive to uracil, though less than wild-type RutR but, remarkably, the inhibitory effect of thymine was strongly enhanced and similar to the effect of uracil (Fig. 2d and e). An enhanced sensitivity for thymine was not observed with RutR-L74A, used as a control (Fig. 2f). RutR-L74A proved to be partially desensitized for uracil, but yet remained insensitive to thymine. Combined these results indicate that the residues Leu74, Trp77; Leu 78 and Trp167 contribute to ligand binding but that Leu78 plays a crucial role in ligand specificity, allowing the binding of uracil but discriminating against thymine.

2.3. Effects of single alanine substitutions in RutR on positive regulation of carP1 expression

To determine the impact of the W77A, L78A and W167A substitutions on RutR-mediated stimulation of *car*P1 activity, we used a

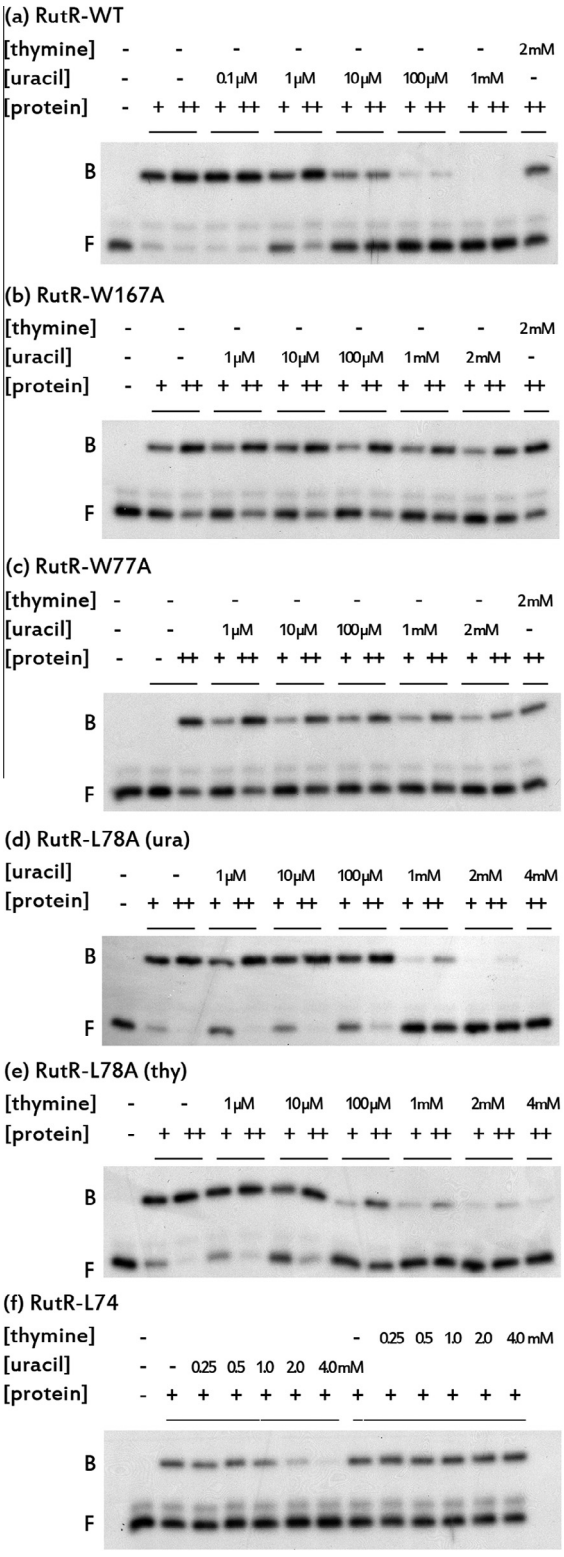

Fig. 2. Representative autoradiographs of EMSAs with the binding of purified wild type and mutant RutR proteins to a 116 bp fragment carrying the RutR binding site of the *car*P1 control region in the absence (−) and in the presence of uracil and thymine (final concentrations as indicated). Protein–DNA complexes were separated by gel electrophoresis on 6% polyacrylamide. Binding of (a) wild type RutR, (b) RutR-W167A, (c) RutR-W77A, (d) and (e) RutR-L78A, (f) RutR-L74A. The positions of free (F) DNA and of protein–DNA complexes (B) are indicated. + and ++ (double amount as compared to +) indicate the protein concentrations used in the different lanes.

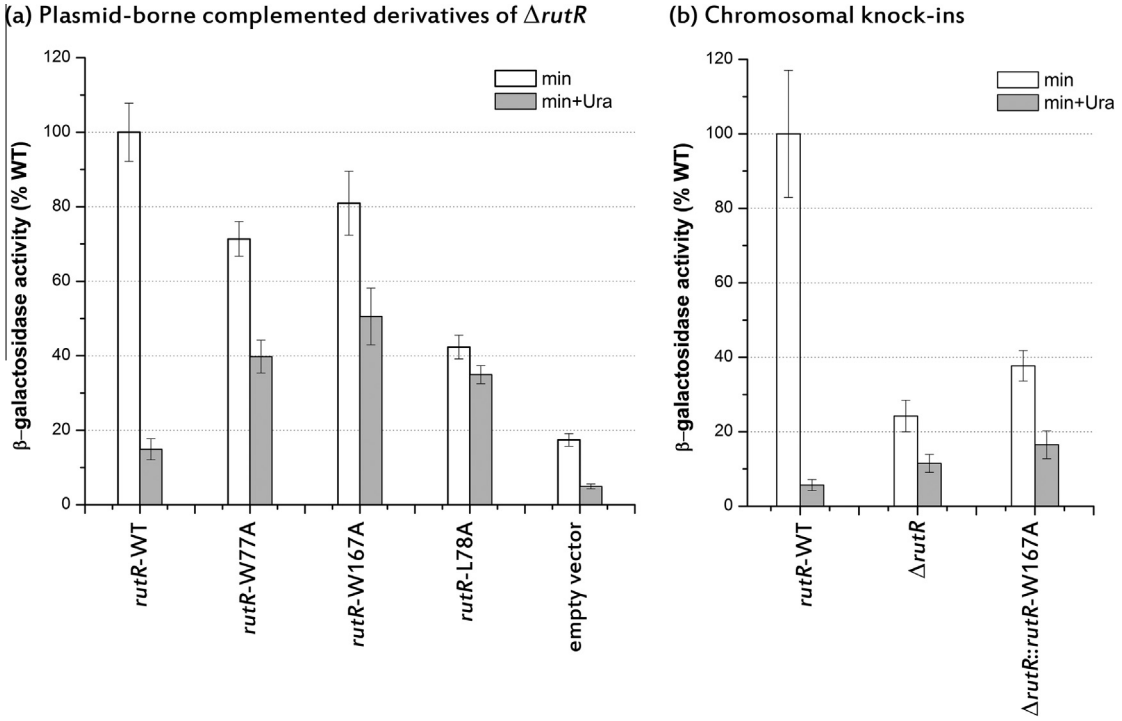

Fig. 3. Histogram presentation of β-galactosidase activities measured in cell-free extracts of strains carrying the *car*P1-*lacZ* reporter fusion on single copy episome F′-carP1. Cells were grown on minimal medium (min) and uracil-supplemented minimal medium (min + ura) and harvested at exponential growth phase. Values are the means ± standard deviations (error bars) of at least three independent assays (biological replicates). (a) Activities of *E. coli* strain FW102 Δ*rutR* complemented with low-copy number plasmid pACYC184 carrying either wild type *rutR* or a single amino acid mutant *rutR* allele (pACYC-rutR-W77A, pACYC-rutR-L78A or pACYC-rutR-W167A). Empty vector indicates transformation with vector pACYC184 without insert. The 100% corresponds to the activity measured in the *rutR* deletion strain complemented with wild type *rutR* on the plasmid grown on minimal medium. (b) Activities measured in cell-free extracts of strain FW102Δ*rutR* and knock-in derivatives carrying either wild type *rutR* or the W167A mutation (Δ*rutR*::*rutR*-W167A). The 100% corresponds to the activity measured in the wild type *rutR* knock-in grown on minimal medium.

single-copy *car*P1-*lacZ* reporter construct (F′-carP1) and assayed β-galactosidase activity in cultures of strain FW102Δ*rutR*/F′-carP1 complemented with a wild type or mutant *rutR* allele present on low-copy number vector pACYC184, grown with and without uracil supplementation (Fig. 3a). The results indicate that complementation of the Δ*rutR* strain with wild-type *rutR* results in an approximately sixfold stimulation of *car*P1 activity on minimal medium as compared to complementation with the empty vector used as a control, and a twofold increase in the down-regulation by uracil (Fig. 3a). In the three Δ*rutR* derivatives complemented with a mutant *rutR* allele (W77A, L78A, or W167A), *car*P1 activity was somewhat lower on minimal medium as compared to the wild type complemented strain but remarkably less repressible by uracil. The W77A and W167A substitutions resulted in a 1.5 and 1.3-fold drop, respectively, of *car*P1 activity on minimal medium and the effect of uracil supplementation was reduced to 1.8- and 1.6-fold, respectively, as compared to the 7.3-fold observed with wild-type *rutR* complementation. The negative effect of uracil supplementation on *car*P1 activity is even smaller in the alanine substitution mutants than in the absence of *rutR* (complementation with empty vector). Therefore, we may conclude that the RutR-mediated effect of uracil supplementation has completely vanished in the W77A and W167A mutants. Similarly, *car*P1 activity in the L78A mutant was strongly reduced and nearly constitutive (1.2-fold decrease with uracil only). Curiously, the *rutR*-L78A complemented strain showed an extended lag phase on minimal medium, but not on uracil supplemented medium. The reasons for this behaviour are not known. Combined our results indicate that all three alanine substitutions affect RutR-mediated stimulation of *car*P1 activity at low pyrimidine concentrations in the cell to a various extent, and most importantly render this activation potential insensitive to uracil supplementation.

To further validate these observations we constructed a single-copy *rutR*-W167A knock-in mutant by substituting the mutant allele for the Δ*rutR* deletion on the chromosome, and assayed *car*P1 activity with the F′-borne reporter construct (Fig. 3b). The results indicate that *car*P1 activity in the *rutR*-W167A mutant is about 2.7-fold lower than in the wild type strain on minimal medium and again, the reduction upon uracil supplementation is slightly below the effect of uracil observed in the Δ*rutR* mutant (Fig. 3b). This complete relief of RutR-mediated uracil-specific inhibition of *car*P1 activity corroborates our results obtained with the plasmid borne *rutR*-W167A construct.

2.4. Effects of single alanine substitutions in RutR on negative autoregulation

Previously, uracil supplementation was shown to result in an enhanced *rutR* promoter activity [9]. To further analyse this potential negative autoregulation and the impact of the W167A substitution on this process, we constructed the episome-borne reporter gene construct F′-p/o-*rutR*, in which *lacZ* expression is put under control of the *rutR* promoter/operator, and introduced this construct in various genetic backgrounds. The results indicate that RutR exerts negative autoregulation in a uracil-sensitive manner, and that this effect of uracil has vanished in the *rutR*-W167A mutant (Fig. 4a). Previously RutR was shown to bind to the control region of the divergent *rutR*-*rutABCDEFG* gene cluster [9,12] and it was suggested that a single binding site, situated downstream of the start site of *rutR* transcription might be used to control both wings of the cluster (Fig. 5) [9]. To investigate the importance of this binding site in autoregulation, we constructed an O^C derivative of the episome borne p/o-*rutR*-*lacZ* reporter gene fusion bearing four bp substitutions in the 15 bp RutR target site (Fig. 5).

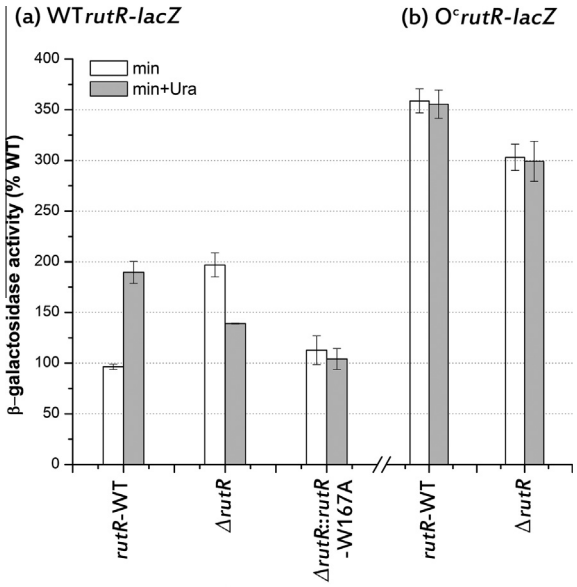

Fig. 4. Histogram presentation of β-galactosidase activities measured in cell-free extracts of derivatives of strain FW102 Δ*rutR* carrying the wild type *rutR* promoter/operator-*lacZ* reporter fusion or the operator constitutive derivative *rutR*-O^c-*lacZ* fusion on a single copy F′ episome. Cells were grown on minimal medium (min) and uracil-supplemented minimal medium (min + ura) and harvested at exponential growth phase. Values are the means ± standard deviations (error bars) of at least three independent assays (biological replicates). (a) Activities measured in cell-free extracts of strain FW102Δ*rutR* bearing the wild type *rutR* promoter-operator-*lacZ* reporter gene fusion and knock-in derivatives of FW102Δ*rutR* carrying either wild type *rutR* or the W167A mutation. (Δ*rutR*::*rutR*-W167A). The 100% corresponds to the activity measured in the wild type *rutR* strain grown on minimal medium. (b) As in (a) but with the operator constitutive *rut-O^c-lacZ* reporter gene fusion. The 100% corresponds to the activity measured with the episome borne wild type fusion in the wild type *rutR* strain grown on minimal medium (see panel (a)).

Combined, the β-galactosidase assays indicate that this site, situated in an unusual position, downstream of the transcription initiation site of *rutR*, is indeed required for negative and uracil-sensitive autoregulation (Figs. 4b and 5).

2.5. Structure determination of unliganded RutR-W167A

To overcome the high affinity of RutR for uracil and in order to obtain a structure of apo-RutR, we crystallized the mutant W167A protein, which as shown above is severely hampered in the binding of uracil, and determined its structure at 2.4 Å resolution (Table 1) in the absence of the effector uracil. RutR-W167A has the same fold as the wild type protein (Fig. 6a) with a r.m.s.d for superimposition of 2.05 Å (Fig. 6c), while the two uracil-bound forms deposited in the PDB (3LOC and 4JYK) are more similar to each other, with a r.m.s.d. of 1.03 Å. Both uracil-bound RutR structures show an open conformation incompatible with DNA binding [14], with a distance

Table 1
Data collection and refinement statistics.*

Data collection	RutR-W167A
Beamline	Xaloc (ALBA)
Wavelength (Å)	0.97946
Space group	$P2_12_12_1$
Unit cell *a*, *b*, *c* (Å)	48.42 91.77 97.71
Resolution range (Å)	66.89–2.40
(Highest resolution shell)	(2.53–2.40)
Total reflections	61,883 (8848)
Unique reflections	17,045 (2485)
I/σ_I	6.2 (2.1)
R_{sym}† (%)	8.7 (33.2)
Completeness (%)	97.2 (98.6)
Redundancy	3.6 (3.6)
$CC_{1/2}$	99.6 (92.9)
Wilson B factor (Å^2)	21.8
Refinement	
Resolution range (Å)	66.89–2.40
Reflections (work/test)	16,147/865
R factor‡ (work/test) (%)	19.62/24.89
Number of:	
Polypeptide chains	2
Protein atoms	3093
Water	91
Average B-factors (Å^2)	
Protein atoms	58.94
Water	48.65
RMSD bond (Å)	0.01
RMSD angle (°)	1.31
Ramachandran plot§	
Favored (%)	99.5
Allowed (%)	0.5
Outliers (%)	0.0
Molprobity score (overall percentile)§	1.22 (100)

* Values in parenthesis are data for the highest resolution shell.
† $R_{sym} = \Sigma|I - \langle I\rangle|/\Sigma I$, where *I* is the observed intensity, and <*I*> is the average intensity of multiple observations of symmetry-related reflections.
‡ *R* factor = $\Sigma_{hkl}||F_{obs}|-|F_{calc}||/\Sigma_{hkl}|F_{obs}|$, where F_{obs} and F_{calc} are the observed and calculated structure factors, respectively.
§ Calculated using Molprobity server (http://molprobity.biochem.duke.edu/).

between the two recognition α3 helices (the main element in binding of RutR to the major groove of operator DNA) of 48.3 and 46.2 Å for 4JYK and 3LOC, respectively (measured as the distance between the Cα atoms of Leu56 of each subunit). An analysis of all DNA-bound structures of members of the TetR family (14 structures deposited in the PDB belonging to 11 different regulators) shows that binding of DNA requires a closed conformation of the regulator, with distances between the residues equivalent to Leu56 in the range of 34.5 Å for ms654 (PDB: 4JL3) to 39.5 Å for SlmA (PDB: 4GCK) (average value of 36.86 Å) [4].

The RutR-W167A structure, despite of not having uracil in its binding site (Fig. 6d), shows an open conformation, with a distance between both α3 helices of 44.1 Å (Fig. 6a), lower than that in the uracil-bound RutR structures but still too large for being suited for

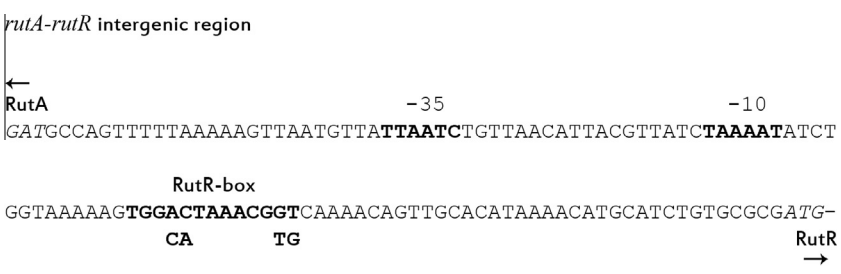

Fig. 5. DNA sequence of the *rutR-rutABCDEFG* intergenic region. Arrows indicate the direction of *rutR* and *rutABCDEFG* transcription. The initiation codon of RutR and RutA (complementary strand) are indicated in italics. The −10 and −35 *rutR* promoter elements are indicated in bold. The conserved 15 bp sequence of the RutR binding site (RutR-box) in the intergenic region is indicated in bold and the four bp substitutions introduced in the operator constitutive derivative are indicated below the sequence.

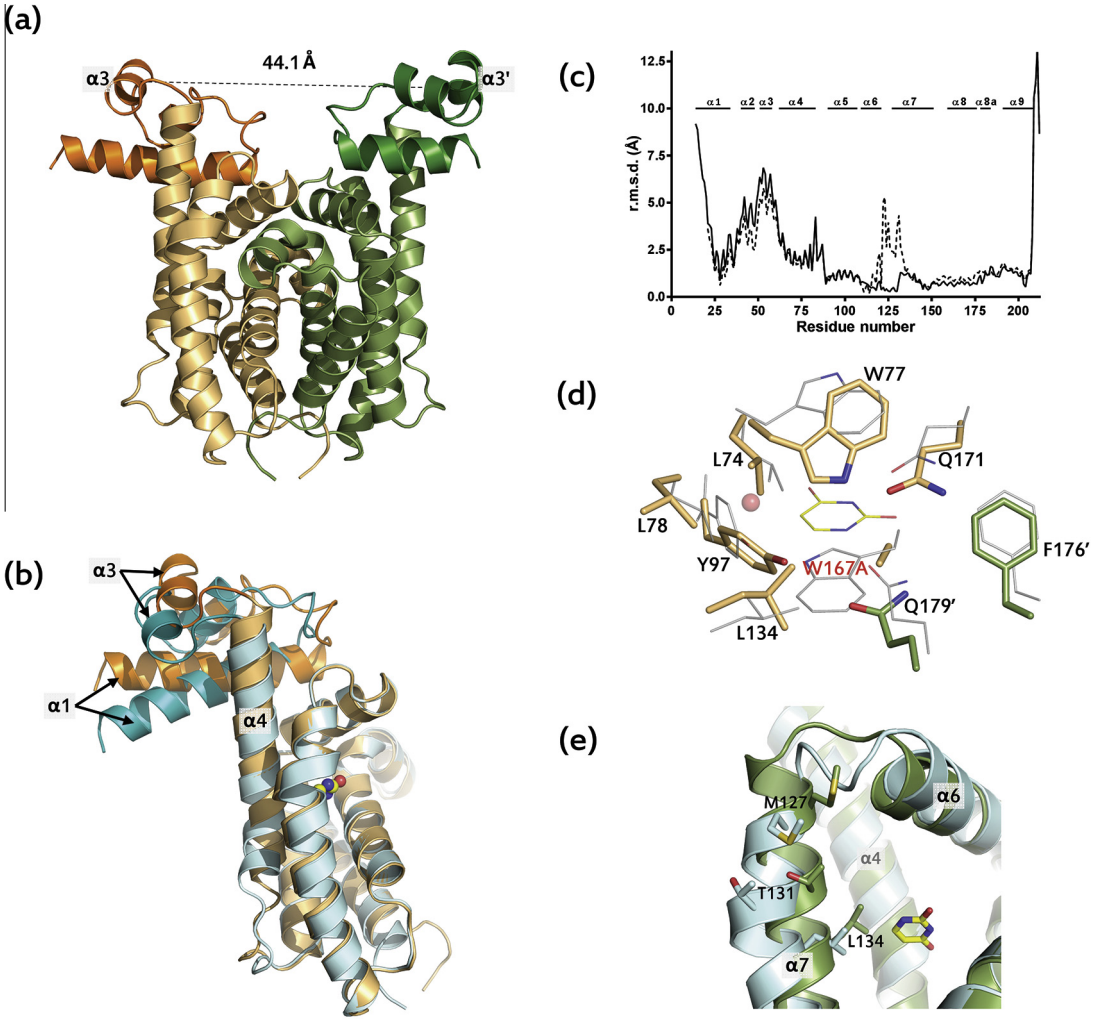

Fig. 6. Structure of RutR-W167A mutant. The uracil-containing structure used for comparisons was taken from PDB4JYK. (a) Cartoon representation of RutR mutant W167A. Each subunit is coloured in two different hues of the same colour (orange or green) to identify its two domains. The dashed line and number (in Å) on top indicates the distance between both α3 helices, which are labelled. (b) Rotation of the DBD with respect to the LBD and displacement of helix α4. The structures of one subunit of the uracil-bound (cyan) and of the W167A mutant (orange) are superimposed through their LBD domains. Helices α1, α3 and α4 are labelled to highlight their movements. Uracil from the wild type structure is shown in spheres representation. (c) Plot versus residue number of the r.m.s.d. values for superimposition of the structures of the LBDs of subunit A (continuous line) or B (dashed line) of the W167A mutant with the structure of the A subunit of the wild type protein. The locations and spans of the α helices along the sequence are indicated (top horizontal bars). (d) Uracil binding site in the W167A mutant structure. Residues are shown in sticks representation from with C atoms coloured in orange for one subunit and in green for the adjacent subunit. The superimposed binding site of the uracil-bound form is also shown with thinner lines and protein C atoms coloured grey. (e) Detailed view of the structural change in the α6–α7 connection observed in subunit B of the W167A mutant (green) superimposed with the uracil bound structure (cyan). Some residues are shown in sticks to highlight the different orientation due to structural changes. (For interpretation of the references to colour in this figure legend, the reader is referred to the web version of this article.)

DNA binding. The DNA-binding domains of TetR family members are relatively flexible in their apo-form (higher B-factors for residues in this domain are usually observed, also for RutR, Fig. 6c) allowing them to adopt the conformation required for DNA binding [15], while the binding of the effector results in the stiffening of the protein in the open, ineffective DNA-binding form. Therefore, it is not uncommon that apo TetR family members do not crystallize in their DNA-binding form, as observed for CgmR, SimR, SlmA and TetR itself [4], but in a conformation where, due to its flexibility, their α3 helices are too separated to be able to bind two successive major groove segments aligned on the same face of the target DNA.

However, the crystal structure of the W167A mutant protein provides evidence of the inter-domain communication that is predicted to be required for the transmission of the effector-binding signal to the DBD. Superimposition of uracil-bound wild type and W167A mutant RutR structures shows that the dimerization interface (helices α8 and α9) and the conserved central triangle observed in all TetR family members (helices α5-α7) [4] keep the same conformation in both forms (Fig. 6b and c). Binding of uracil to the allosteric site requires a reorientation of the side chain of Trp77, so that the aromatic ring of uracil gets stacked between the side chains of Trp77 and Trp167 (Fig. 6d). This reorientation is associated to a displacement of up to 2.4 Å of the N-terminal part of helix α4 (that bears Trp77) and a transition from 3_{10}- to α-helix of the last five C-terminal residues of this helix (residues 78–83) (Fig. 6b). These changes are somehow reminiscent of the ones observed in HrtR, where a coil-to-helix transition in the middle of helix α4 upon binding of the effector (haem) produces a rigid body motion of the DBD to an orientation incompatible with the binding of DNA [16]. The consequence of the structural changes in helix α4 of RutR is a 18° rigid body rotation of the DBD with respect to the ligand binding domain (Fig. 6b), with the hinge located in the middle zone of helix α4, resulting in a displacement of up to 9 Å of the first residues of helix α1, and of 6 Å for helix α3. These results suggest that helix α4 is a key structural component in the transmission of the uracil-dependent allosteric signal from the

ligand-binding pocket to the DBD, and therefore in the control of the ability of RutR to bind DNA.

An additional structural change is observed only in one subunit (subunit B) of the W167A mutant RutR protein. This subunit shows also a transition upon uracil binding, from coil to helix, in a small insertion in helix α7 (Gly132), introducing therefore an extra turn to the helix and altering the conformation of the preceding α6–α7 connecting loop (Fig. 6e). This change in the apo-structure is probably mediated by the lack of hydrophobic interaction between the aromatic ring of uracil and the side chain of Leu134, which allows Leu134 to penetrate the binding site, thereby altering the continuity of helix α7 in the uracil-bound form.

3. Discussion

The availability of two high-resolution structures of uracil-bound RutR (3LOC and 4JYK) allowed us to identify the effector-binding site and to test for the importance of particular amino acid residues in effector binding and specificity by site directed mutagenesis.

Similar to TetR, the archetype of the family, and many other family members, RutR possesses two symmetric effector-binding sites in the functional dimer (Fig. 1a). In contrast, QacR that shows high sequence conservation with RutR in the DNA-binding domain and was used to build a model of the RutR-carP1 operator interactions [12], is asymmetric with only one of the subunits binding the effector and undergoing the structural changes that render the regulator unable to bind DNA [17]. QacR binds mono- and bivalent cationic lipophilic drugs as effector molecules and regulates transcription of the MDR pump [18,19].

As all TetR-like regulators, RutR shows a binding site that is rich in aromatic and hydrophobic residues (Fig. 1a and b). Here we show that the tryptophan residues W77 and W167 and the hydrophobic leucine residue L74 play an important role in binding of the planar ring-shaped uracil molecule that abolishes the DNA binding capacity of the regulator. In a previous report by Shimada et al., thymine was proposed to exert a similar negative effect on DNA binding [9]. However, in the same concentration range we did not observe this negative effect of thymine on complex formation [12]. A close inspection of the effector-binding site of RutR and modelling of the hydrophobic methyl group of thymine on the bound uracil molecule of the co-crystal rather suggests a steric clash of the methyl group with the side chain of leucine residue L78 (Fig. 1d). This hypothesis is corroborated by the result of our mutagenesis study. DNA binding of RutR-L78A proved to be as sensitive to thymine as to uracil, whereas, in contrast, the wild type protein and all other mutant proteins studied in this work are much more sensitive to uracil than to thymine. Therefore, we may conclude that leucine residue L78 plays a crucial role in setting the effector specificity of RutR. These observations indicate that RutR has a very narrow effector binding specificity, unlike the broad substrate specificity exhibited by many other TetR-family members, in particular the ones that are involved in regulation of multidrug resistance mechanisms [3,4]. Interestingly, the PydR regulator that represses the pyrimidine reductive pathway in *Pseudomonas putida* and its homologs from *Brucella suis* and *Sinorhizobium meliloti* show striking amino acid sequence conservation of all the residues involved in uracil binding, including L74, W77 and W167 [20]. Similarly, leucine residue L78 is conserved in PydR from *B. suis* and *S. meliloti*, suggesting that these two regulators, which are globally more similar to *E. coli* RutR than to *P. putida* PydR, might exhibit the same narrow effector specificity as RutR. In *P. putida* PydR, however, the equivalent position bears a lysine residue, which could potentially allow the binding of both uracil and thymine.

As all TetR-family members, RutR undergoes an allosteric transition upon binding of its effector molecule uracil that results in abrogation of its DNA binding activity [9,12]. However, unlike most family members that repress transcription in the apo-form, RutR both represses and activates transcription. In the absence of uracil supplementation, RutR exerts negative autoregulation and represses the divergently transcribed *rutABCDEFG* operon by binding to a single RutR box in the intergenic region [9]. But, RutR also exerts a positive effect on the *car*P1 promoter of the *carAB* operon through binding to a RutR box centred around position −184.5, far upstream of the start of *car*P1 transcription [12]. The underlying mechanism of this positive control has not been elucidated yet, but the position of the RutR box in the *car*P1 control region suggests an anti-repression strategy rather than a direct stimulation of RNA polymerase binding. Shimada et al. [9] suggest an interference of RutR with the binding of PepA to the *car*P1 control region, but this has not been confirmed. Only few examples of positive control by TetR-members have been documented. DhaS from *Lactococcus lactis*, activates transcription of the *dha* operon by binding to a palindromic target site that partially overlaps the predicted −35 promoter sequence [21]. Interestingly, DhaS uses the dihydroxyacetone-binding protein DhaQ as a macromolecular inducer and co-activator instead of a small ligand, as do all other characterized members of the TetR repressor family. Another example of positive control is LuxR, the master quorum-sensor regulator from the marine bacterium *Vibrio harvey* that acts both as a repressor and an activator of several genes [22].

RutR was previously shown to exert negative regulation on both wings of the divergently transcribed *rutR-rutABCDEFG* gene cluster. Here we demonstrate that negative autoregulation involves a 15 bp conserved RutR box located downstream of the RNA polymerase binding site (Fig. 5). This site, located upstream of the *rutA* promoter, was previously proposed to be involved in RutR mediated repression of the *rutABCDEFG* operon that is transcribed from a σ^{54} promoter and regulated by NtrC, the general regulator of nitrogen metabolism [1]. The exact mechanism by which RutR exerts autoregulation is not known but this less common position of the regulator binding site suggest a regulatory mechanism distinct from direct competition with the RNA polymerase for DNA binding. Regulators binding downstream of the start site of transcription have been shown to exert negative regulation by inhibiting the isomerization of the open to the closed complex, the transition from the initiating to the elongating complex, or to work as a roadblock for the elongating polymerase [23]. In view of the short distance separating the initiation site from the RutR box, the latter hypothesis appears to be improbable.

Several different mechanisms of derepression by effector binding have been proposed for the TetR family members. These include a shift of helix α6 and a pendulum-like movement of helix α4 in TetR [24], a coil to helix transition in helix α5 and relocation of helix α6 in QacR [13], a coil to helix transition in helix α4 in HrtR [16], or even a rigid body rotation of both subunits relative to each other in SimR [25]. Ideally, a DNA-bound structure would allow us to identify the precise changes induced by the binding of uracil to RutR that lead to dissociation of RutR-DNA complexes. However, the analysis of the apo-RutR-W167A structure allows us to identify some structural transitions, mainly a 3_{10}-to α-helix transition in helix α4 and a small transition in helix α7, that turn into a rigid body movement of the DNA binding domain with relation to the ligand binding domain. These observations allow us to predict that the mechanism of induction of RutR must be in some way similar to those observed in QacR or HrtR, although the changes necessary for RutR to bind the operator DNA must be of a larger magnitude than those described here.

4. Materials and methods

4.1. Plasmid constructions and site-directed mutagenesis

All oligonucleotides used in this work were obtained from Sigma and are listed in Supplemental data (Table S1). Plasmids pFW11-null [26], pFW-carP1 [27] and pET24-rutRHis6 [12] are described. Low copy number plasmid pACYC184 was obtained from New England Biolabs and pET24a from Novagen. Plasmids pKD46 [Red helper plasmid, Ap^r], pKD3 (containing an FRT-flanked chloramphenicol resistance (*cat*) gene) and pCP20 (expressing FLP recombinase) are described [28] and were obtained from Prof. Dr. Jean-Pierre Hernalsteens. Plasmid pFW-p/o-rutR was constructed by amplification of the *rutR* control region with the oligonucleotides DC1061f and DC818r and ligation of the EcoRI and BamHI digested amplicon in similarly digested pFW11-null vector. The operator constitutive derivative $rutRO^c$ was constructed with the overlap extension method [29] using the oligonucleotides DC1076f and DC1077r as primers. To construct low copy-number plasmid pACYC-rutR, the *rutR* coding and control region was amplified with the oligonucleotides DC1444f and Rv-rutR-EcoRI, digested with EcoRI, and ligated into the EcoRI site of pACYC184. The mutant derivatives pACYC-rutR-W77A, pACYC-rutR-L78A and pACYC-rutR-W167A, bearing a single alanine substitution mutation, were obtained with the overlap extension method using the oligonucleotides DC994f and DC995r (W77A), DC1002f and DC1003r (L78A) and DC996f and DC997r (W167A) as primers. The same strategy was used to construct the single alanine substitution mutants of expression vector pET24-rutRHis6. Similarly, the oligonucleotides DC998f and DC999r were used to insert the L74A substitution. All constructs were verified by DNA sequencing.

4.2. E. coli strains and growth conditions

E. coli MG1655 [λ^-, F^-, *rph*-1, *rfb*-50, *ilvG*$^-$, *fnr*$^-$] was obtained from the Netherlands Culture Collection of Bacteria (NCCB, Utrecht, The Netherlands). The genotypes and construction of *E. coli* strains DH5α, CSH100 (F′), FW102 (F^-) and FW102/F′-carP1 are described [26,27]. FW102Δ*rutR* was constructed by deleting the coding part of *rutR* on the chromosome of strain FW102 with the one-step inactivation method based on the λ Red recombinase, described by Datsenko and Wanner [28] with the oligonucleotides Fw-rutR-P1 and Rv-rutR-P2 as primers. To obtain a marker-less deletion mutant the *cat* gene was removed by FLP-mediated recombination of the flanking FRT sites, and finally the strain was cured of plasmid pCP20 upon growth at 42 °C. The *rutR*-W167A knock-in mutant was generated by λ Red mediated homologous recombination of a *rutR*-W167A-*cat* fusion in the FW102Δ*rutR*/pKD46 background, using the strategy described by Datsenko and Wanner [28].

4.3. Electrophoretic mobility shift assays (EMSA)

EMSA experiments were performed with 116 bp long (−127 to −244 with respect to the start of *car*P1 transcription) 5′-single end labelled PCR amplicons, as described [12]. Amplicons were generated with as primers the oligonucleotides DC663f and DC664r, one of which was 5′-end labelled, and pFW-carP1 plasmid DNA as template.

4.4. β-Galactosidase assays

β-Galactosidase specific activities were assayed in cell-free extracts of cultures grown in minimal medium 132 [30] supplemented with glucose, vitamin B1, appropriate antibiotics for plasmid or episome bearing strains, and uracil when indicated. Cells were harvested by centrifugation of chilled cultures in the exponential growth phase at a density of 4×10^8 cells ml^{-1}. Assays were performed as described by Miller [31]. Values are the means of at least three independent assays.

4.5. Overexpression and purification of wild type and mutant RutR proteins

C-terminally hexa-histidine tagged wild type and mutant RutR proteins were purified from 900 ml cultures of strain BL21(DE3) transformed with plasmid pET-*rutR*His6 for the wild type protein, and mutant versions thereof, bearing the corresponding single alanine substitution for the mutant proteins. Cultures were grown at 30 °C in medium 132 supplemented with 0.5% glucose, 1 μg ml^{-1} thiamine, and 60 μg ml^{-1} kanamycin. When cell density reached 6×10^8 cells ml^{-1}, the culture was induced with isopropyl-β-d-thiogalactopyranoside (IPTG) at 1 mM and grown overnight.

The purification scheme was based on previously described protocol [9]. Briefly, lysate obtained from sonicated harvested cells was filtered by 0.45 μm syringe filter (Sarstedt) prior to loading onto a HisTrapFF column (GE Healthcare) allowing Ni^{2+} ion affinity chromatography purification of the His-tagged protein. Equilibration of the column was performed with 20 mM sodium phosphate buffer, 0.5 M NaCl, 40 mM imidazole pH 7.4. Elution of RutR-His_6 was obtained by applying a linear gradient from 40 to 500 mM imidazole. Fractions containing RutR-His_6 protein were identified by SDS–PAGE and mobility shift assays with the *carAB* operator region as probe. Fractions containing RutR-His_6 at a degree of purity >95% were pooled and were submitted to dialysis against the storage buffer, 20 mM Tris–HCl pH 7.6, 200 mM KCl, 10 mM $MgCl_2$, 1 mM EDTA, 1 mM DTT and 12.5% glycerol.

4.6. Crystallization, data collection and structure determination of RutR-W167A

Crystallization screenings of mutant RutR-W167A protein were performed by the sitting-drop vapour diffusion method in 96-well MRC plates using a HoneyBee X8 robot (Genomic Solutions). An equal volume of the protein solution at 10 mg ml^{-1} in a buffer containing 20 mM Tris–HCl pH 7.6, 200 mM KCl, 10 mM $MgCl_2$, 1 mM EDTA and 1 mM dithiotreitol was mixed with an equal volume of screening solution. The plates were stored at 21 °C. The best crystal, having plate-like appearance, was obtained in a condition with 20% (w/v) methanol, 10 mM $CaCl_2$ and 0.1 M Tris–HCl pH 8.5. The crystals were harvested and flash-cooled in liquid nitrogen using 30% glycerol as cryoprotectant.

Diffraction images were collected with a Dectris PILATUS3 6M detector at beamline Xaloc of the ALBA synchrotron source (Barcelona, Spain) using a wavelength of 0.97 Å at 100 K. The data were indexed and integrated using iMosflm [32]; the intensities were calculated and merged with SCALA [33] and converted to structure factors with TRUNCATE [34]. The crystals diffracted to a resolution of 2.40 Å and belonged to the primitive orthorhombic space group $P2_12_12_1$. The unit cell parameters (a = 48.42 Å; b = 91.77 Å and c = 97.71 Å) were consistent with two RutR subunits in the asymmetric unit. A summary of the diffraction data and refinement statistics is presented in Table 1.

The structure was solved by molecular replacement with PHASER [35] using the wild type RutR structure (PDB 3LOC) as search model. After an initial rigid body refinement with the two domains of RutR the model was optimized in several cycles of refinement with jelly-body and non-crystallographic symmetry restraints using REFMAC5 [36] and graphical model building with Coot [37]. Waters were manually incorporated in the final stages of modelling, and isotropic B factors and TLS were used in the last steps of refinement. Throughout the refinement process 5% of the diffraction data were used for R_{free} calculations. Molprobity [38]

and PDB_REDO [39] were used to monitor and improve the stereochemistry of the final model. The DynDom server was used to calculate rotation angles between domains (http://fizz.cmp.uea.ac.uk/dyndom/) and figures were generated with PyMol (http://sourceforge.net/projects/pymol/).

PDB accession numbers

The atomic coordinates and structure factors of RutR-W167A have been deposited to the wwPDB under the accession code PDB: 4X1E.

Author contributions

P.N.L.M., S.D.C., I.B. and D.C. conceived and performed the experiments. P.N.L.M., S.D.C., I.B. and D.M. contributed to structural data analyses. P.N.L.M., S.D.C. and D.C. drafted the manuscript. I.B., D.M. and V.R. revised the paper.

Acknowledgements

The authors acknowledge the excellent technical assistance of Nadine Huysveld (Brussels) and Nadine Gougeard (Valencia). X-ray diffraction studies were performed at the Xaloc beamline at the ALBA/CELLS synchrotron with the collaboration of ALBA staff. The authors acknowledge financial support from: Research Foundation Flanders (FWO-Vlaanderen) [G.0429.06 to D.C., a postdoctoral fellowship to P.N.L.M., and a stay abroad to P.N.L.M.]; Research Council of the Vrije Universiteit Brussel (OZR-VUB); Vlaamse Gemeenschapscommissie; Spanisch Government [BFU2011-30407]; Valencian Government [Prometeo II/2014/029]; Instituto de Salud Carlos III-CIBERER [contract to S.D.C.].

Appendix A. Supplementary data

Supplementary data associated with this article can be found, in the online version, at http://dx.doi.org/10.1016/j.fob.2015.01.002.

References

[1] Loh, K.D., Gayaneshwar, P., Papadimitriou, E.M., Fong, R., Kwang-Seo, K., Parales, R., Zhou, Z., Inwood, W. and Kustu, S. (2006) A previously undescribed pathway for pyrimidine catabolism. Proc. Natl. Acad. Sci. U.S.A. 103, 5114–5119.
[2] Aramaki, H., Yagi, N. and Suzuki, M. (1995) Residues important for the function of a multihelical DNA binding domain in the new transcription factor family of Cam and Tet repressors. Protein Eng. 8, 1259–1266.
[3] Ramos, J.L., Martínez-Bueno, M., Molina-Henares, A.J., Terán, W., Watanabe, K., Zhang, X., Gallegos, M.T., Brennan, R. and Tobes, R. (2005) The TetR family of transcriptional repressors. Microbiol. Mol. Biol. Rev. 69, 326–356.
[4] Yu, Z., Reicheld, S.E., Savchenko, A., Parkinson, J. and Davidson, A. (2010) A comprehensive analysis of structural and sequence conservation in the TetR family transcriptional regulators. J. Mol. Biol. 400, 847–864.
[5] Cuthbertson, L. and Nodwell, J.R. (2013) The TetR family of regulators. Microbiol. Mol. Biol. Rev. 77, 440–475.
[6] Deng, W., Li, C. and Xie, J. (2013) The underlying mechanism of bacterial TetR/AcrR family transcriptional repressors. Cell Signal. 25, 1608–1613.
[7] Berens, C. and Hillen, W. (2003) Gene regulation by tetracycline. Constraints of resistance regulation in bacteria shape TetR for application in eukaryotes. Eur. J. Biochem. 270, 3109–3121.
[8] Gossen, M., Freundlieb, S., Gender, B., Muller, G., Hillen, W. and Bujard, H. (1995) Transcriptional activation by tetracyclines in mammalian cells. Science 268, 1766–1769.
[9] Shimada, T., Hirao, K., Kori, A., Yamamoto, K. and Ishihama, A. (2007) RutR is the uracil/thymine-sensing master regulator of a set of genes for synthesis and degradation of pyrimidines. Mol. Microbiol. 66, 744–757.
[10] Kim, K.-S., Pelton, J.G., Inwood, W.B., Andersen, U., Kustu, S. and Wemmer, D.E. (2010) The Rut pathway for pyrimidine degradation: novel chemistry and toxicity problems. J. Bacteriol. 192, 4089–4102.
[11] Shimada, T., Ishihama, A., Busby, S.J.W. and Grainger, D.C. (2008) The *Escherichia coli* RutR transcription factor binds at targets within genes as well as intergenic regions. Nucleic Acids Res. 36, 3950–3955.
[12] Nguyen Le Minh, P., Bervoets, I., Maes, D. and Charlier, D. (2010) The protein–DNA contacts in RutR·*carAB* operator complexes. Nucleic Acids Res. 38, 6286–6300.
[13] Schumacher, M.A., Miller, M.C., Grkovic, S., Brown, M.H., Skurray, R.A. and Brennan, R.G. (2002) Structural basis for cooperative DNA binding by two dimers of the multidrug-binding protein QacR. EMBO J. 21, 1210–1218.
[14] Itou, H., Watanabe, N., Yao, M., Shirakihara, Y. and Tanaka, I. (2010) Crystal structures of the multidrug binding repressor *Corynebacterium glutamicum* CgmR in complex with inducers and with an operator. J. Mol. Biol. 403, 174–184.
[15] Reicheld, S.E., Yu, Z. and Davidson, A.R. (2009) The induction of folding cooperativity by ligand binding drives the allosteric response of tetracycline repressor. Proc. Natl. Acad. Sci. U.S.A. 106, 22263–22268.
[16] Sawai, H., Yamanaka, M., Sugimoto, H., Shiro, Y. and Aono, S. (2012) Structural basis for the transcriptional regulation of heme homeostasis in *Lactococcus lactis*. J. Biol. Chem. 287, 30755–30768.
[17] Schumacher, M.A., Miller, M.C., Grkovic, S., Brown, M.H., Skurray, R.A. and Brennan, R.G. (2001) Structural mechanisms of QacR induction and multidrug recognition. Science 294, 2158–2163.
[18] Grkovic, S., Brown, M.H., Roberts, N.J., Paulsen, I.T. and Skurray, R.A. (1998) QacR is a repressor protein that regulates expression of the *Staphylococcus aureus* multidrug efflux pump QacA. J. Biol. Chem. 273, 18665–18673.
[19] Grkovic, S., Brown, M.H., Schumacher, M.A., Brennan, R.G. and Skurray, R.A. (2001) The *Staphylococcal* QacR multidrug regulator binds a pair of correctly spaced operators as a pair of dimers. J. Bacteriol. 183, 7102–7109.
[20] Hidese, R., Mihara, H., Kurihara, T. and Esaki, N. (2012) *Pseudomonas putida* PydR, a RutR-like transcriptional regulator, represses the dihydropyrimidine dehydrogenase gene in the pyrimidine reductive catabolic pathway. J. Biochem. 152, 341–346.
[21] Christen, S., Srinivas, A., Bahler, P., Zeller, A., Pridmore, D., Bieniossek, C., Baumann, U. and Erni, B. (2006) Regulation of the Dha operon of *Lactococcus lactis*: a deviation from the rule followed by the TetR family of transcription regulators. J. Biol. Chem. 281, 23129–23137.
[22] Pompeani, A.J., Irgon, J.J., Berger, M.F., Bulyk, M.L., Wingreen, N.S. and Bassler, B.L. (2008) The *Vibrio harveyi* master quorum-sensing regulator, LuxR, a TetR-type protein is both an activator and a repressor: DNA recognition and binding specificity at target promoters. Mol. Microbiol. 70, 76–88.
[23] Yang, J., Camakaris, H. and Pittard, J. (2002) Molecular analysis of tyrosine- and phenylalanine-mediated repression of the *tyrB* promoter by the TyrR protein of *Escherichia coli*. Mol. Microbiol. 45, 1407–1419.
[24] Orth, P., Schnappinger, D., Hillen, W., Saenger, W. and Hinrichs, W. (2000) Structural basis of gene regulation by the tetracycline inducible TetR repressor-operator system. Nat. Struct. Biol. 7, 215–219.
[25] Le, T.B., Schumacher, M.A., Lawson, D.M., Brennan, R.G. and Buttner, M.J. (2011) The crystal structure of the TetR family transcriptional repressor SimR bound to DNA and the role of a flexible N-terminal extension in minor groove binding. Nucleic Acids Res. 39, 9433–9447.
[26] Whipple, F.W. (1998) Genetic analysis of prokaryotic and eukaryotic DNA-binding proteins in *Escherichia coli*. Nucleic Acids Res. 26, 3700–3706.
[27] Devroede, N., Thia-Toong, T.L., Gigot, D., Maes, D. and Charlier, D. (2004) Purine and pyrimidine-specific repression of the *Escherichia coli carAB* operon are functionally and structurally coupled. J. Mol. Biol. 336, 25–42.
[28] Datsenko, K.A. and Wanner, B.L. (2000) One-step inactivation of chromosomal genes in *Escherichia coli* K12 using PCR products. Proc. Natl. Acad. Sci. U.S.A. 97, 6640–6645.
[29] Higuchi, R., Krummel, B. and Saiki, R.K. (1988) A general method for *in vitro* preparation and specific mutagenesis of DNA fragments: study of protein and DNA interactions. Nucleic Acids Res. 16, 7351–7367.
[30] Glansdorff, N. (1965) Topology of cotransducible arginine mutations in *Escherichia coli* K-12. Genetics 51, 167–179.
[31] Miller, H.J. (1972) Experiments in Molecular Genetics, Cold Spring Harbor Laboratory Press, Cold Spring Harbor, NY.
[32] Battye, T.G.G., Kontoggianis, L., Johnson, O., Powell, H.R. and Leslie, A.G.W. (2011) IMOSFLM: a new graphical interface for diffraction-image processing with MOSFLM. Acta Crystallogr. D: Biol. Crystallogr. 67, 271–281.
[33] Evans, P.R. (2006) Scaling and assessment of data quality. Acta Crystallogr. D: Biol. Crystallogr. 62, 72–82.
[34] French, S. and Wilson, K. (1978) On the treatment of negative intensity observations. Acta Crystallogr. A: Found. Crystallogr. 34, 517–525.
[35] Mc Coy, A.J., Grosse-Kunstleve, R.W., Adams, P.D., Winn, M.D., Storoni, L.C. and Read, R.J. (2007) Phaser crystallographic software. J. Appl. Crystallogr. 40, 658–674.
[36] Murshudov, G.N., Skubák, P., Lebedev, A.A., Pannu, N.S., Steiner, R.A., Nicholls, R.A., Winn, M.D., Long, F. and Vagin, A.A. (2011) REFMAC5 for the refinement of macromolecular crystal structures. Acta Crystallogr. D: Biol. Crystallogr. 67, 355–367.
[37] Emsley, P., Lohkamp, B., Scott, W.G. and Cowtan, K. (2010) Features and development of Coot. Acta Crystallogr. D: Biol. Crystallogr. 66, 486–501.
[38] Chen, V.B., Arendall III, W.B., Headd, J.J., Keedy, D.A., Immormino, R.M., Kapral, G.J., Murray, L.W., Richardson, J.S. and Richardson, D.C. (2010) MolProbity: all-atom structure validation for macromolecular crystallography. Acta Crystallogr. D: Biol. Crystallogr. 66, 12–21.
[39] Joosten, R.P., Salzemann, J., Bloch, V., Stockinger, H., Berglund, A.C., Blanchet, C., Bongcam-Rudlmoff, E., Combet, C., Da Costa, A.L., Deleage, G., Diarena, M., Fabbretti, R., Fettahi, G., Flegel, V., Gisel, A., Kasam, V., Kervinen, T., Korpelainen, E., Mattila, K., Pagni, M., Reichstadt, M., Breton, V., Tickle, I.J. and Vriend, G. (2009) PDB_REDO: automated refinement of X-ray structure models in the PDB. J. Appl. Crystallogr. 42, 376–384.